A New Two-Site Model for Hydroxyapatite Dissolution in Acidic Media[1]

JEFFREY L. FOX,[2] WILLIAM I. HIGUCHI, MAHDI B. FAWZI, AND MAW-SHENG WU

College of Pharmacy, The University of Michigan, Ann Arbor, Michigan 48109

Received October 7, 1977; accepted May 30, 1978

A physical model featuring two distinct types of dissolution sites for hydroxyapatite (HAP) crystals is presented. One of these sites (site No. 1) is associated with dissolution along *c* axis dislocations of HAP crystals and is the important site when dissolution occurs into partially saturated solutions. Site No. 2 is active only when dissolution occurs into nearly completely unsaturated solutions, and, because of its greater apparent rate constant, is the more important dissolution site under these conditions.

In the physical model block dental enamel or a compressed HAP pellet is represented as a porous matrix of these HAP crystals with interstitial spaces which are permeated by the dissolution medium. The behavior of the model for various situations can be calculated by combining Fick's second law equation for diffusion with the kinetic equations for the behavior of the dissolution sites and solving the resulting boundary value problem.

This model is capable of accounting for dissolution kinetics over a range of variation of experimental variables (degree of undersaturation, Ca/P ratio, and effective diffusion layer thickness). The model also correctly predicts the conditions necessary for zonal as opposed to surface dissolution: high partial saturation, a viscous dissolution medium, or the presence of a site No. 2 dissolution inhibitor. Electron microscopic studies of dissolution morphology at the single crystal level are also in full agreement with the model.

Finally, an examination of the available data on enamel remineralization suggests that the holes formed as a result of site No. 1 dissolution are likely the primary sites for remineralization.

Because of its clinical importance, the dissolution behavior of dental enamel and of hydroxyapatite has been the focus of attention of many investigations (1–9). Until recently, a quantitative explanation of many of the aspects of enamel and hydroxyapatite dissolution behavior has been very elusive, however. We will now present a model involving two distinct dissolution sites which offers an explanation for many of the peculiar features of enamel and hydroxyapatite behavior, and in addition is capable of quantitatively describing the dissolution kinetics over a wide range of conditions. We will begin by describing how the model has been used to study the dissolution kinetics of hydroxyapatite; in so doing we will also discuss some other possible interpretations that are kinetically indistinguishable from this two-site model. We will then cite other kinds of experimental evidence that strongly supports the two-site hypothesis. Finally, we will discuss the potential benefits to be gained from the thorough characterization of hydroxyapatite and tooth enamel via this physical modeling approach.

REVIEW

Production of carious lesions has long been associated with an attack of the enamel by various acids produced by the bacteria of the mouth (10–16). A simple model (1) was

[1] This investigation supported by NIDR grants DE-01830 and DE-04600.

[2] To whom correspondence should be addressed.

0021-9797/78/0672-0312$02.00/0

developed about 1965 to attempt to explain the acid attack of enamel and of hydroxyapatite, the mineral component of tooth enamel, in various acidic media. In this model, hydroxyapatite was assumed to follow the classical Noyes–Whitney model for the diffusion controlled dissolution of a solid (17). Although extremely simple in concept, this model enjoyed notable success in explaining dissolution rate behavior of both hydroxyapatite and tooth enamel under conditions of low or zero partial saturation.

There were some difficulties with this early model, however. First, the solubility product of hydroxyapatite ($Ca_{10}(PO_4)_6(OH)_2$) was thought to be about 10^{-115}, and the best fit of the model to a large number of experiments indicated that the effective driving force for dissolution corresponded to an ion activity product of only about 10^{-124}–10^{-125}. Second, the model failed to explain the clinically observed morphology of a caries lesion: dissolution occurring not from the surface, but from a zone extending from the surface to a depth of perhaps 50 μm. This zonal dissolution was observed clinically as the formation of opaque "white spots" on the tooth. These spots possessed significantly less hardness than the surrounding enamel.

Examination of sectioned carious lesions using polarized light, transmitted light, and micro radiography (18–20) had indicated an area near the surface of the tooth that appeared intact, and some investigators (21) proposed that zonal dissolution occurred primarily because this intact outer layer had a much lower solubility in the acidic media presumed to be responsible for caries formation. This idea was refuted as the sole explanation for white spot formation when Gray and Frances (22, 23) and Sperber and Buonocore (24) demonstrated that white spots could be formed on blocks of enamel which had the surface layer removed by grinding. Zonal dissolution thus appeared to be a property of the bulk enamel itself, and not an experimental anomaly resulting from the presence of a less soluble intact outer layer. In fact, this zonal dissolution has been observed in our laboratory even with pellets of synthetic hydroxyapatite crystals.

THE MATRIX MODEL FOR HYDROXYAPATITE DISSOLUTION

Since zonal dissolution was a property of human teeth, but not of the powdered hydroxyapatite systems used in the early dissolution rate studies, an experimental system was designed that more closely simulated the geometry of a tooth. Instead of studying suspensions of hydroxyapatite crystals, the crystals were now compressed into a porous pellet, which was mounted in a rotating disk apparatus (25, 26). Use of the rotating disk system also permitted a quantitative estimation of the effective diffusion layer thickness, h, according to the equation of Levich (27):

$$h = 1.612 D^{1/3} \nu^{1/6} \omega^{-1/2}$$

where D = diffusivity, ν = kinematic viscosity, and ω = angular velocity. The mineral region of the system is viewed as a porous matrix of hydroxyapatite crystals, with intercrystalline spaces that are readily permeated by the bulk solution. The effective diffusivity, D_i', of the ith species in this region is given by

$$D_i' = D_i \frac{\epsilon}{\tau} \cdot f \qquad [1]$$

where D_i is the aqueous diffusivity of the ith species, ϵ and τ are porosity and tortuosity of the matrix region, and f is the constriction factor.

The concentration of the ith species in the matrix region obeys Fick's second law diffusion equation modified for the production of the ith species by solution reactions and by crystal solvation:

$$\frac{\partial C_i}{\partial t} = D_i' \frac{\partial^2 C_i}{\partial x^2} + \phi_{i,\text{soln}} + \phi_{i,\text{solv}} \qquad [2]$$

where

C_i = concentration of the ith species at point x,
$\phi_{i,\text{soln}}$ = rate of production of ith species by solution reactions, and
$\phi_{i,\text{solv}}$ = rate of production of ith species due to crystal solvation.

It has been shown (28) that when the D_i' are equal and the steady-state is assumed, that these equations can be combined to give a single equation that describes the system:

$$D' \frac{d^2C}{dx^2} + R = 0 \qquad [3]$$

where

C = concentration of hydroxyapatite at point x,
D' = diffusivity of all species in the matrix region, and
R = the rate of solvation of crystalline hydroxyapatite at x.

For the case where R is a first order expression, an analytic solution is readily obtained. The case where R is an arbitrary function has been described elsewhere (28).

To simplify the computational work, and for lack of any compelling reasons for choosing another functional form, R was assumed to be first order with respect to undersaturation, that is:

$$R = k(C_s - C).$$

The geometry of the model is shown in Fig. 1. The boundary conditions for Eq. [3] which applies to the region $x \leq 0$, can now readily be written. If C_s is the solubility of hydroxyapatite in the bulk solution, then $C \to C_s$ as $x \to -\infty$, and this is the boundary condition for $x \to -\infty$. From this, it also follows that $dC/dx \to 0$ as $x \to -\infty$. At $x = 0$ the flux, F, of hydroxyapatite from the matrix region is given by

$$F = -D' \frac{dC}{dx}. \qquad [4]$$

Consideration of the region $0 \leq x \leq h$

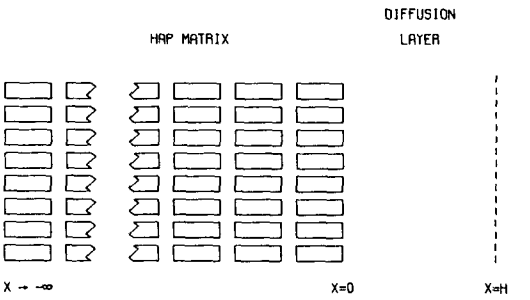

FIG. 1. Schematic of geometry of HAP matrix dissolution model.

yields another expression for the flux of hydroxyapatite, namely:

$$F = \frac{D}{h}(C_0 - C_h) \qquad [5]$$

where

D = aqueous diffusivity,
C_0 = concentration of hydroxyapatite at $x = 0$, and
C_h = concentration of hydroxyapatite at $x = h$.

Equating these two flux expressions yields a boundary condition for $x = 0$.

Solving the differential equation along with the boundary conditions yields an expression for the flux:

$$F = \frac{C_s - C_h}{\frac{h}{D} + \frac{1}{(kD')^{1/2}}}. \qquad [6]$$

Note that as k gets larger, this expression reduces to the usual expression for diffusion-controlled dissolution. The real value of this expression lies in the fact that everything except C_s and $(kD')^{1/2}$ can either be measured directly or estimated fairly closely. The effective diffusion layer thickness, h, can be calculated from hydrodynamic considerations as already mentioned.

In the early experiments with this system, F was measured as a function of h, and plots made of h/D versus $1/F$. The slope of such a plot, $C_s - C_h$, enabled the calculation of the K_{sp} corresponding to the apparent solubility driving force for dissolution. The

intercept, $-(kD')^{1/2}$, permitted an estimation of the magnitude of the first order kinetic rate constant, k. These early experiments invariably involved solutions that were completely unsaturated, although some calcium or phosphate (not both) may have been present. For several sets of solution conditions, experiments conducted over a range of disk rotation speeds gave essentially the same conclusion (25): the apparent K_{sp} of hydroxyapatite, deduced from dissolution data, was about 10^{-125}. This conclusion was similar to that reached by Higuchi and his co-workers in the mid-1960s.

The fact that the apparent K_{sp} measured during dissolution was not identical with the thermodynamic K_{sp} was a source of considerable consternation. This need not have been so, however. A plot of the rate, R, of hydroxyapatite crystal solvation versus undersaturation, $C_s - C$, as deduced from these early experiments (and assuming the linear functional form) is shown in Fig. 2. Figure 3 shows typical plots for this same quantity as generated by computer simulation studies for a model solid (29). Curve I, a straight line through the origin, is characteristic of a solid with rapid dissolution kinetics, while curve III is for a solid with slower kinetics. From this, then, it would appear that these early dissolution experiments done in solutions with a high degree of undersaturation correspond to the linear region of curve III. Operationally, then, if not physically, it was convenient to regard hydroxyapatite dissolution kinetics under these conditions as being governed by a "dissolution site" having an "apparent solubility" corresponding to an ion product, $a_{Ca}{}^{10} a_{PO_4}{}^{6} a_{OH}{}^{2}$, equal to 10^{-125} (25).

The obvious next set of experiments would be those designed to "fill in the gap" in the curve shown in Fig. 2. Many experiments in this range of undersaturation were carried out, and the results of these experiments, too, were well described by the matrix dissolution model with the first order kinetic function. This time, however, the kinetic constant, k, was much smaller and the "apparent solubility" corresponded to an ion activity product of 10^{-120} (30).

There are several interpretations possible at this point. One that immediately suggests itself is the existence of two distinct types of dissolution site on the hydroxyapatite crystal, each having properties as depicted in Fig. 2, with one site having an apparent solubility corresponding to an ion product of 10^{-120}, the other to 10^{-125}. Another possibility is that there is only one type of site, but that there are two parallel mechanisms operating.

If we add the R versus $C_s - C$ functions for the two sites or mechanisms together to give a total R versus $C_s - C$ curve as in Fig. 4, a third possibility suggests itself: only one site, only one mechanism, but a complicated rate law corresponding to the total R dependency.

THE DUAL-MECHANISM MODIFICATION TO THE MODEL

Up to this point the rate of solvation has been assumed to be governed by the linear kinetic function:

$$R = k(C_s - C)$$

where k and C_s are the kinetic rate constant and "apparent solubility" associated with the governing dissolution mechanism. Since experimental evidence points to the existence of more than one mechanism (or at least a mechanism sufficiently complex to be indistinguishable from the sum of two simpler ones), the following was proposed as a possible rate law:

$$R = k_1(C_{s1} - C) + k_2(C_{s2} - C)$$

where the ks and C_ss are the same as before, each associated with one of the two apparent mechanisms. To be consistent with the previous treatments, a site or mechanism is assumed to be operating only when C is less than the corresponding C_s. Although the terminology used to this point

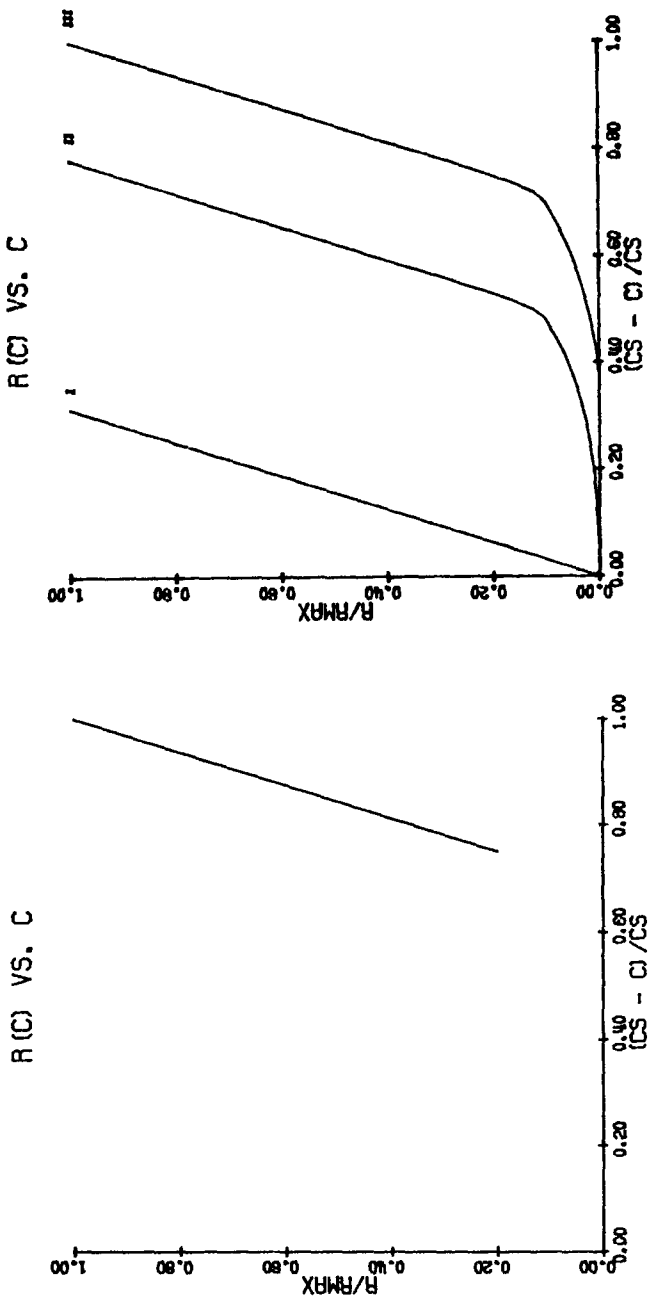

FIGS. 2 and 3. Microscopic solvation rate (R) at crystal surface vs undersaturation. Fig. 2, for hydroxyapatite, as deduced from dissolution experiments; Fig. 3, simulated rates for model solid.

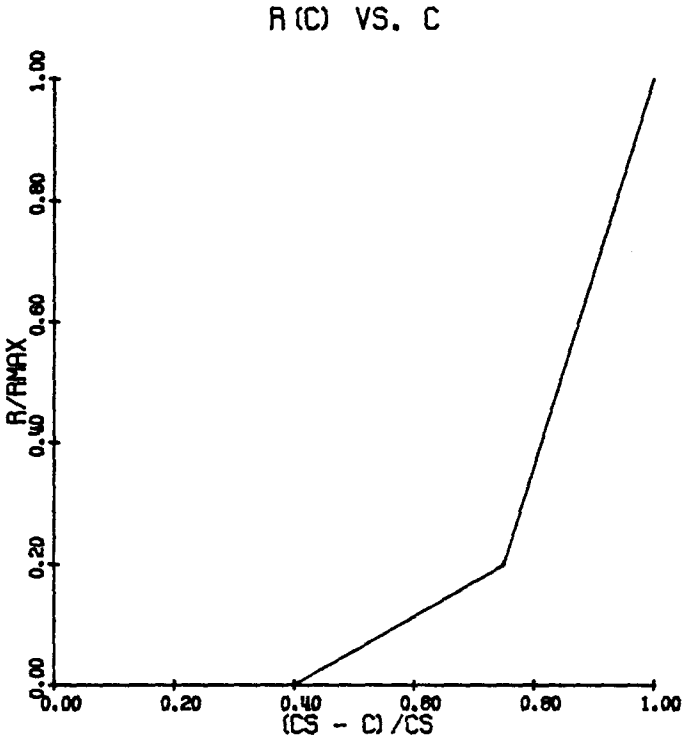

FIG. 4. Solvation rate vs undersaturation for dual-mechanism or two-site case.

is more applicable to the case where the model involves dual sites or mechanisms, it is clear that the values of the ks and C_ss obtained in any fitting procedure could be used equally well to characterize the two segments of a bilinear approximation to a more complicated single mechanism such as is shown in Fig. 4. At this point we shall examine this model more closely to test its ability to describe the existing experimental data.

DATA FITTING WITH THE MODEL

Although the model is general and intended for application to dissolution under nearly any reasonable experimental conditions, the present discussion will be limited to experiments carried out in 0.1 N acetate buffer at pH 4.5 under sink conditions and moderate partial saturation conditions (25, 30).

As already mentioned h/D vs $1/F$ plots were used in previous studies to determine the values of C_s and k associated with a given set of solution conditions. These values could then be converted to the more manageable parameters, K_{HAP}, which is the ionic activity product that would prevail if C_s moles of hydroxyapatite were dissolved in 1 liter of the bulk solution, and k', which is defined as $(kD')^{-1/2}$.

Using a nonlinear least squares technique and the mathematics shown in Appendix I, the model was fit to the available dissolution rate data. The following were the questions to be answered by the fitting procedure:

1. Assuming the first order kinetic rate law for each site or mechanism, is a single site or mechanism for dissolution sufficient to describe the data, or must more than one site or mechanism be employed?

2. What are the best estimates for the model parameters?

In order to answer these questions, nonlinear least squares fitting procedures were

carried out for both the single-mechanism and dual-mechanism models with several different subsets of the experimental data (28). This fitting led to the following conclusions:

1. The dissolution rate data for HAP pellets in 16% partially saturated solutions (30) was explainable with a single-mechanism model with the driving force corresponding to an activity product of $10^{-119.9}$ and the kinetic parameter, k', equal to about 1250 [recall $k' = (kD')^{-1/2}$] as shown in Fig. 5.

2. This 16% partial saturation data and data (25) obtained under sink conditions (0% partial saturation) could not be simultaneously fit with the single-mechanism model (28). The dual-mechanism or two-site model, however, did an excellent job of simultaneously fitting these data sets.

3. Inclusion of data obtained under conditions of 4, 6, and 8% partial saturation constitutes a severe test of the model. The most satisfactory fit when all these sets of data were considered [and the effective diffusivity of 1.0×10^{-5} cm^2/sec measured by Wu (25) was used] is shown in Fig. 6. The discrepancy of about 15% between the 0% curve and the 0% experimental data is indicative of either the functional form used in the model not being exactly correct or of the effective diffusivity being incorrect.

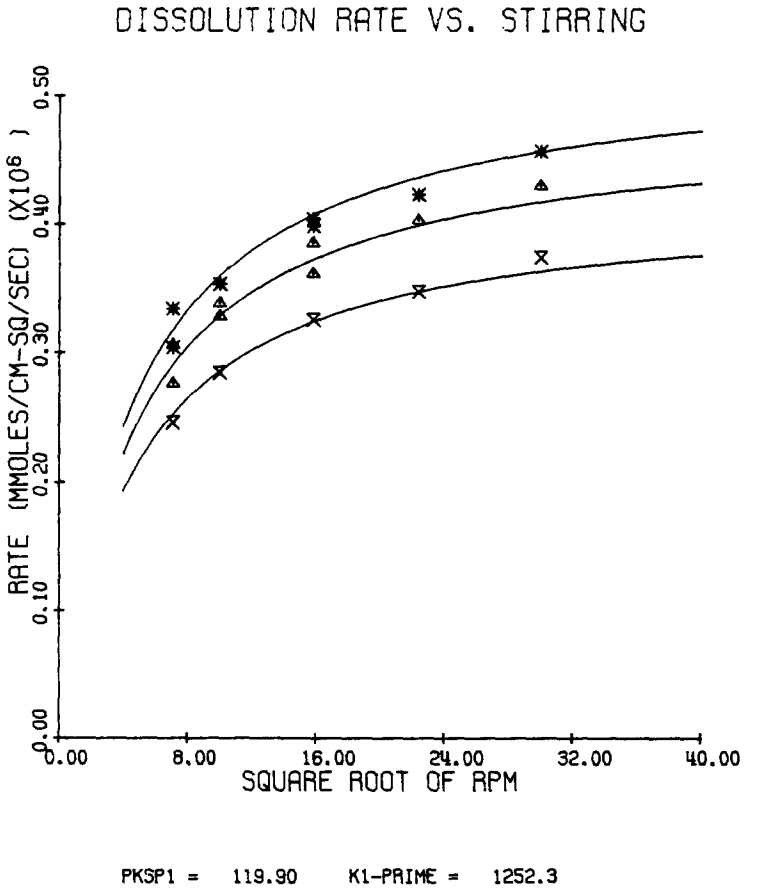

FIG. 5. Best fit of one-site model to dissolution in 16% partially saturated solutions at pH 4.5. Top to bottom, curves represent Ca/P ratios of 1:1, 10:1, and 1:10. Symbols are experimental points, solid lines are calculated from model.

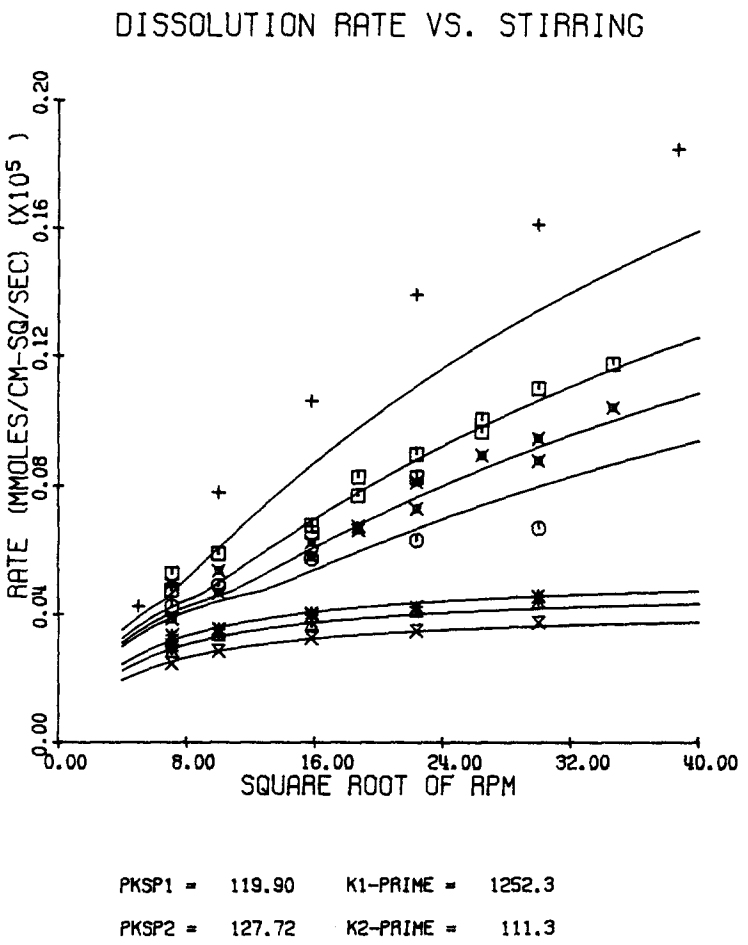

FIG. 6. Best fit of two-site model to all data, assuming $D = 1.0 \times 10^{-5}$. Top to bottom, curves and symbols represent solutions with partial saturations of 0, 4, 6, and 8% with Ca/P ratios of 1:1 and 16% with Ca/P ratios of 1:1, 10:1, and 1:10.

4. Since the mobilities of the various species as estimated from published conductance data suggested that an effective diffusivity of about 1.4×10^{-5} cm²/sec might be appropriate for this system, the fitting procedure was repeated using a higher value for diffusivity to see if such a change in diffusivity would affect the ability of the model to fit the data. As seen in Fig. 7, setting the diffusivity equal to 1.5×10^{-5} cm²/sec allowed the model to give a very close fit to all the sets of data, representing a total of over 40 sets of experimental conditions.

Regardless of which value is most appropriate for the effective diffusivity, the main conclusion of the fitting procedures is that the dissolution data are not explainable by a single-site model, but is readily explainable by a two-site model. Since the main theme of this communication is simply to demonstrate the existence of two dissolution sites, we will not further pursue the diffusivity issue at this time.

THE PHYSICAL VALIDITY OF THE TWO-SITE MODEL

Thus far we have indicated how previous studies of dissolution kinetics led us to the two-site model for hydroxyapatite dissolu-

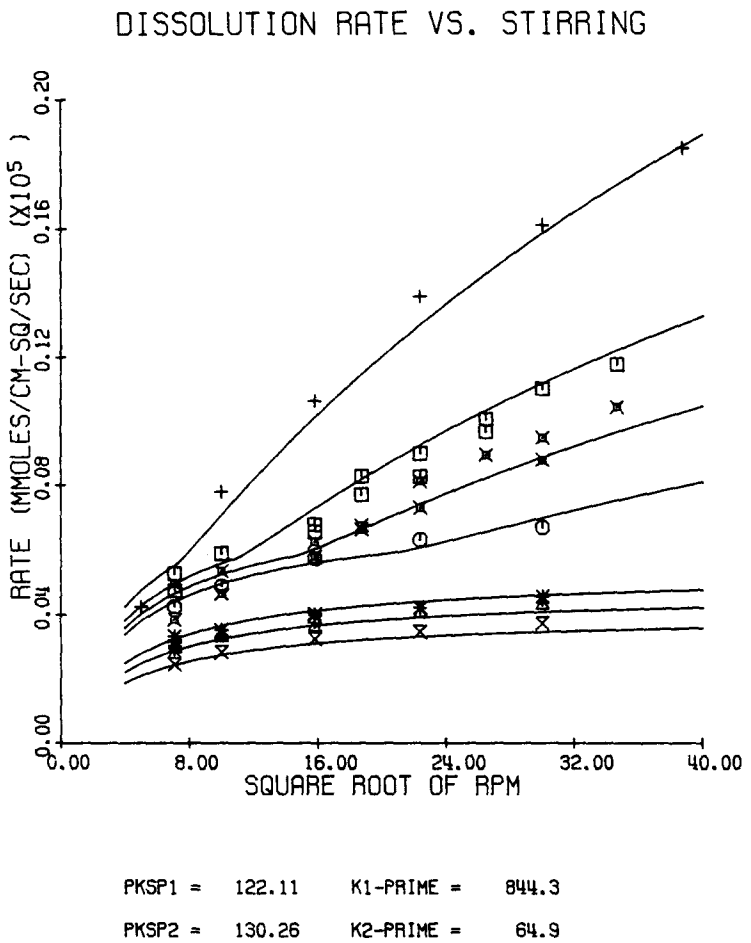

FIG. 7. Best fit of two-site model to all data, assuming $D = 1.5 \times 10^{-5}$. Top to bottom, curves and symbols represent solutions with partial saturations of 0, 4, 6, and 8% with Ca/P ratios of 1:1 and 16% with Ca/P ratios of 1:1, 10:1, and 1:10.

tion. We have also noted that the kinetic studies are incapable of differentiating among the following possibilities:

1. Two independent dissolution sites
2. One site with two independent mechanisms
3. One site with one mechanism having a complicated rate law.

To choose among them, other types of experimental observations must be considered.

In the case of hydroxyapatite, there is an abundance of evidence in support of the idea of two dissolution sites. We have previously discussed how studies of dissolution kinetics and the observations of zonal dissolution contributed to the idea of the two-site model. We shall now review the results of both morphological studies and remineralization studies, and then describe the logical extension of the dissolution model to encompass a wider range of situations, such as tooth remineralization and maturation.

MORPHOLOGICAL STUDIES

The idea that enamel crystals might have two distinct types of dissolution sites was initially inspired by two unrelated sets of studies.

1. Gallily and Friedlander (31) had postulated a mechanism for ferric ion inhibition of the dissolution of lithium fluoride crystals that clearly implied the existence of two types of sites for dissolution, although they did not attempt to characterize the kinetics of the two sites.

2. Several investigators (32–34) had done SEM studies on the etching of enamel by acids and by EDTA and had clearly shown morphological differences at the prism level. It was shown that EDTA attacked chiefly at the periphery of the enamel prisms (32–34) while the acids attacked primarily at the prism centers (33, 34). The fact that enamel prisms were attacked at different sites by acid and EDTA along with the observation that a crystal as simple as the cubic lithium fluoride had more than one type of dissolution site, led us to hypothesize that enamel crystals, too, could have more than one type of dissolution site.

Many more direct morphological studies strongly support the existence of two dissolution sites. Scott and his co-workers (35, 36) observed that enamel crystals both in carious lesions and *in vitro* dissolved by forming a hole along the *c*-axis, leading to a hollow shell which eventually fragments if the dissolution process continues long enough. It had been postulated earlier (37) that the centers of the crystals might be comprised of a different phase than the outer shells. If this were the case it would be quite natural to associate two types of dissolution sites with these crystals.

That this anisotropic dissolution of enamel crystallites which had also been observed by others (33, 37, 38) did not necessarily imply the existence of two phases was at least suggested by work done by Poole (39). Working with large fluorapatite crystals, he showed that the etch patterns were different on the various faces, although the dissolution rates did not vary significantly from face to face.

A more definitive study of the anisotropic dissolution of fluorapatite and hydroxyapatite single crystals was done by Arends *et al.* (40). They studied flawless gem quality fluorapatite crystals and found a definite anisotropy in the rates of etch pit penetration parallel and perpendicular to the *c* axis, with the rate parallel to the *c* axis being a factor of 10 greater at 60°. Crystals of hydroxyapatite were also studied, and showed an even greater anisotropy, the ratio being about 100 to 1. These workers also showed that hydroxyapatite dissolution begins at a single screw-like etch pit in the basal plane. This was attributed to a screw dislocation along the *c* axis (41), and hence was consistent with ideas that many others had put forth regarding defects or weak spots in the centers of hydroxyapatite crystals (36, 42–45).

More recently, work done in our laboratories (46) has shown that when hydroxyapatite crystals are subjected to dissolution under partial saturation conditions such that only site No. 1 of our model is presumed operating, holes result similar to those seen by Scott and Arends. On the other hand, crystals which are subjected to dissolution under sink conditions, presumed to occur mainly via site No. 2 of our model, show no such fully developed holes, but only tiny "pinpoint-like" beginnings of holes (46). These results clearly indicate that the two kinetic sites of our model are, in fact, physically distinct dissolution sites.

REMINERALIZATION STUDIES

The kinetics of the remineralization process has been the subject of several investigations. These investigations with softened enamel showed that the rate of hardness recovery was greater at higher pH values (47), and that at a given pH the rate was linearly related to the concentrations of calcium and phosphate (48). It was also shown that fluoride ion increased the rate of rehardening (49). Interestingly, the enamel samples used in these investigations were typically softened under fairly mild demineralization conditions (50–52) which

would be predicted to give dissolution only from site No. 1 of our two-site model.

It has been proposed that the repeating cycle of demineralization of relatively soluble material, followed by remineralization of less soluble material, is a likely mechanism of enamel maturation (52). The plausibility of this idea is enhanced by the observation that remineralized enamel is as resistant to acid attack as natural enamel, and, furthermore, if the enamel is remineralized in the presence of fluoride, it is more resistant to attack (48).

Recently, studies were initiated in these laboratories to test the hypothesis, suggested by some of the above observations, that material removed from site No. 1 is readily replaced by remineralization, but that removed from site No. 2 is not. Preliminary results are in support of this hypothesis but more work will be necessary before it can be definitely affirmed.

THE PROPOSED DEMINERALIZATION/ REMINERALIZATION MODEL AND ITS *IN VIVO* IMPLICATIONS

Drawing on the information already presented as a background, we will now describe the proposed model for the demineralization/remineralization behavior of tooth enamel.

Tooth enamel will be assumed to be composed of a porous matrix of these hydroxyapatite crystals. Although enamel is certainly more complex than this, this fairly simple picture can account for much of the observed dissolution behavior of enamel. For example, the model explains why strong acids remove layers of enamel from the surface *in toto*, while milder demineralization conditions result in removal of material from a zone of enamel perhaps 50 μm deep. In addition this model explains why this general dissolution also occurs when the dissolution medium is highly viscous or when the agitation conditions are very mild (see Appendix II).

A proposed demineralization/remineralization model can be constructed by extending this two-site dissolution model in a way that is consistent with the known morphological and remineralization studies.

First, the morphological studies of the groups of Scott and of Arends led to the hypothesis that under mild dissolution conditions, corresponding to dissolution from site No. 1 of our two-site model, the crystals dissolve along the c axis, probably along a screw dislocation, leading to the formation of holes. Under more severe conditions, corresponding to dissolution from site No. 2, the c axis is shortened (53).

In terms of our model, then, site No. 1 corresponds to the "unwinding" of the crystal, perhaps along a single path. It is reasonable that this sort of dissolution along a defect would occur quite readily, with a relatively small apparent rate constant because of its occurrence from a limited area. Site No. 2 dissolution, perhaps corresponding to gross dissolution over the entire basal plane, would not be expected to occur so readily. However, when conditions are such that this dissolution can occur, it could contribute much more to the overall dissolution rate due to the larger number of sites participating over the entire basal plane. These morphological ideas are entirely consistent with the observed kinetic properties of the two sites.

Consideration of the remineralization data further strengthens these ideas. Successful remineralization has been accomplished, in general, when conditions of the previous demineralization were not too severe. This could mean that the holes produced under mild (site No. 1) demineralization are readily remineralizable, while the more gross basal plane demineralization (site No. 2) is not so easily reversed.

SUMMARY OF EVIDENCE FOR TWO DISSOLUTION SITES

The results of recent investigations in our laboratories and elsewhere, when pieced together, (i) provide the idea that specific sites for demineralization and remineralization should exist for hydroxyapatite and

dental enamel crystallites and (ii) provide cogent arguments for where the principal site might be.

The data we are referring to may be summarized as follows.

a. The two-site model has been able to explain a large body of experimental data obtained in our laboratories and elsewhere on the weak acid demineralization of hydroxyapatite crystals and dental enamel. The experimental parameters already determined for the two-site dissolution model include apparent solubilities for each of the two sites. A very important feature of this model is that only one site, designated as site No. 1, may dissolve in weak acid buffers when the ambient solution is partially saturated (i.e., ~25% with respect to the thermodynamic solubility for hydroxyapatite).

b. Work by Koulourides, Pigman, Feagin, *et al.* on enamel "softening" and "rehardening" has shown that, when enamel is demineralized in weak acid buffers under partial saturation conditions, rehardening by a calcifying solution is rather successful. When demineralization is carried out with a too highly undersaturated weak acid buffer (where both sites are expected to be involved in dissolution according to our model), the results of the rehardening attempts are poor. Also, if the demineralization is conducted for too long a period prior to remineralization, satisfactory rehardening does not take place.

c. Electron microscope studies in several laboratories have shown that hydroxyapatite and enamel crystallites may dissolve by developing holes in the centers of the crystals along the *c* axis. These holes widen with increasing time of dissolution. This phenomenon occurs when weak acid buffers are employed and/or under conditions when the solution bathing the crystals would be expected to be partially saturated (and therefore the second site, site No. 2, is not permitted to contribute to the dissolution). There appears to be no indication that, under these conditions, other crystal morphological changes (such as shortening of the crystals along the *c* axis or dissolution from the external crystal faces) take place up to about 50–70% dissolution.

These results collectively suggest that a principal site for effective remineralization is the site No. 1 of our two-site model for hydroxyapatite and enamel crystallite dissolution and that this site may be directly associated with the *c* axis holes in the weak acid-etched hydroxyapatite crystals.

The ultimate power of an approach of this type arises from the inherent complexity of the system and the long time scales involved in real life processes of both caries development and application of prophylaxis regimens. The complexity of the system makes the intuitive development of anticaries treatments difficult at best. The time scales involved in testing various treatments make the accumulation of meaningful clinical information a sufficiently slow and expensive process so that a premium is placed on the ability to select *a priori* treatments that are likely to be successful. When a model of high enough quality is developed, it will be possible to sit at a computer terminal and simulate in a few minutes experiments that might take months or even years to conduct in the laboratory. Simulations of this type would be an invaluable aid in selecting anticaries regimens for clinical trials.

APPENDIX I

Procedure for Theoretical Calculation of Fluxes from the Parameters of the Model

The general procedure for calculating dissolution rates from a matrix with an arbitrary kinetic rate law describing ion disengagement and solvation was given by Fox (28). However, the simple first order kinetics assumed in this paper for the dissolution sites makes an analytical solution of the problem possible. This appendix will give the derivation of the analytic solution

and, for completeness, outline an efficient algorithm for evaluating the solution.

First, since the model is to be used over a variety of experimental conditions, it is necessary to relate K_{HAP1} and K_{HAP2} to the apparent solubilities, C_{s1} and C_{s2}, of the sites in the bulk solution. It is also necessary to define the variable $C(x)$, which in the model relates to the concentration of hydroxyapatite in solution at point x. Since it is only concentration differences that are of concern here, there exist several operationally acceptable ways of defining $C(x)$. In this discussion, $C(x)$ will be defined as the number of moles of $Ca_{10}(PO_4)_6(OH)_2$ per liter that would have to be added to the bulk solution to give a solution identical to that at point x. Hence $C(x)$ is a concentration difference and as defined here this variable has a value of zero in the bulk solution. C_{s1} and C_{s2}, then, represent the number of moles of hydroxyapatite that would have to be added to the bulk solution to give ion activity products, $a_{Ca}{}^{10}a_{PO_4}{}^{6}a_{OH}{}^{2}$, of K_{HAP1} and K_{HAP2}, respectively. C_{s1} therefore is the calculated solubility of $Ca_{10}(PO_4)_6(OH)_2$ in the bulk solution, assuming the K_{sp} of this solid to be K_{HAP1}. C_{s2} is defined similarly, and these quantities are calculated as a function of the K_{HAPs} as described by Fox (28). Once C_{s1} and C_{s2} are known, the calculation of the dissolution rate can proceed.

The model can be pictured as shown in Fig. 1. The differential equations describing the model are

$$D' \frac{d^2C}{dx^2} + k_1 \cdot (C_{s1} - C) = 0 \quad x \le x_0 \quad [A1]$$

$$D' \frac{d^2C}{dx^2} + k_1 \cdot (C_{s1} - C) + k_2 (C_{s2} - C) = 0 \quad x_0 \le x \le 0 \quad [A2]$$

where D' is the apparent diffusivity of dissolved HAP in the matrix region, k_1 and k_2 are the apparent first order rate constants for the two sites, and C_{s1} and C_{s2} are their apparent solubilities as previously described. For $x < x_0$, C is greater than C_{s2} and hence the second site does not dissolve. For $x_0 < x < 0$, C is less than C_{s2} and both sites dissolve. The point x_0 is where C becomes equal to C_{s2}. The numbering of the sites is chosen such that $C_{s1} > C_{s2}$.

The boundary conditions are the following:

as $x \to -\infty$

$$C \to C_{s1}$$

$$C' \to 0$$

at $x = x_0$

$$C = C_{s2}$$

C' is continuous (this follows from continuity of C'', which follows from continuity of C)

as $x \to 0$ from the left

$$\text{flux} = -D'C'(0) = \frac{D}{h}(C(0) - C(h)). \quad [A3]$$

It will be recalled from the definition of C that $C(h)$ is zero. However, $C(h)$ will be retained in the derivation so that the results will be applicable to other systems where $C(h)$ is nonzero.

The solution of [A1] is

$$C(x) = C_{s1} + q_1 e^{(k_1/D')^{1/2}x} + q_2 e^{-(k_2/D')^{1/2}x} \quad x \le x_0. \quad [A4]$$

From the boundary conditions as $x \to -\infty$ it follows that q_2 must be zero. Applying the first boundary condition at $x = x_0$ gives

$$C_{s2} = C_{s1} + q_1 e^{(k_1/D')^{1/2}x_0}. \quad [A5]$$

Differentiating [A4] and evaluating the expression at $x = x_0$ yields

$$C'(x_0) = q_1 \left(\frac{k_1}{D'}\right)^{1/2} e^{(k_1/D')^{1/2}x_0}. \quad [A6]$$

The solution of [A2] is

$$C(x) = q_3 e^{((k_1+k_2)/D')^{1/2}x} + q_4 e^{-((k_1+k_2)/D')^{1/2}x} + \frac{k_1 C_{s1} + k_2 C_{s2}}{k_1 + k_2} \quad x_0 \le x \le 0. \quad [A7]$$

Now, for sake of brevity, some new constants will be defined:

$$K1 = \left(\frac{k_1}{D'}\right)^{1/2}$$

$$K12 = \left(\frac{k_1 + k_2}{D'}\right)^{1/2}$$

$$G = \frac{k_1 C_{s1} + k_2 C_{s2}}{k_1 + k_2}$$

$$EKX = e^{K12 \cdot x_0}.$$

Now [A7] can be differentiated to give an expression for $C'(x)$:

$$C'(x) = K12 \cdot (q_3 e^{K12 \cdot x} - q_4 e^{-K12 \cdot x}) \qquad x_0 \le x \le 0. \quad [A8]$$

Evaluating [A7] and [A8] at $x = 0$ and substituting into [A3] gives

$$\text{Flux} = -D'K12 \cdot (Q3 - Q4)$$
$$= DH \cdot (Q3 + Q4 + G - CH) \quad [A9]$$

where $Q3$, $Q4$, CH, and DH are q_3, q_4, $C(h)$, and D/h, respectively.

Evaluating [A8] at $x = x_0$ and equating with [A6] gives:

$$C'(x_0) = Q1 \cdot K1 \cdot e^{K1 \cdot x_0}$$
$$= K12 \cdot (Q3 \cdot EKX - Q4/EKX) \quad [A10]$$

where $Q1$ is q_1.

The final condition to be satisfied can be written by evaluating [A7] at $x = x_0$ and setting the result equal to C_{s2}:

$$C_{s2} = Q3 \cdot EKX + Q4/EKX + G. \quad [A11]$$

Now the problem has been reduced to solving Eqs. [A5], [A9], [A10], and [A11] for the constants $Q1$, $Q3$, $Q4$, and x_0. (Recall that EKX is a constant containing x_0.)

This system of equations is not difficult to solve. Begin by eliminating $Q1 \cdot e^{(k_1/D')^{1/2} x_0}$ from Eqs. [A5] and [A10], giving

$$\frac{K1}{K12}(CS2 - CS1) = Q3 \cdot EKX - Q4/EKX. \quad [A12]$$

Now, for simplicity, in subsequent manipulations two new variables are defined:

$$T3 = Q3 \cdot EKX$$

$$T4 = Q4/EKX.$$

Equations [A11] and [A12] can be solved for $T3$ and $T4$, and G can be replaced by its definition, yielding

$$T3 = \frac{K1}{2(K12)^2}(CS2 - CS1) \times (K1 + K12) = Q3 \cdot EKX \quad [A13]$$

$$T4 = \frac{K1 \cdot (CS2 - CS1)}{2 \cdot (K12)^2} \times (K1 - K12) = Q4/EKX. \quad [A14]$$

Hence, $T3$ and $T4$ are expressible in terms of the parameters of the model. The definitions of $T3$ and $T4$ can now be used to eliminate $Q3$ and $Q4$ from Eq. [A9], yielding an equation containing only one unknown, EKX:

$$EKX^2 \cdot T4 \cdot (DH - DK) + EKX \cdot DH \times (G - CH) + T3 \cdot (DH + DK) = 0 \quad [A15]$$

where $DK = D' \cdot K12$.

Letting

$$QA = T4 \cdot (DH - DK)$$

$$QB = DH(G - CH)$$

$$QC = T3 \cdot (DH + DK)$$

the solution to [A16] is

$$EKX = \frac{-QB \pm (QB^2 - 4 \cdot QA \cdot QC)^{1/2}}{2 \cdot QA}. \quad [A16]$$

It is easy to choose which sign in the numerator is appropriate. The value of EKX must be positive from the definition of EKX. By examination it is seen that QB is always positive and QC is always negative. In the case where QA is positive with large magnitude (corresponding to rapid rotation speeds, the situation where both sites are active and for which this model is being derived), it is evident that choosing the positive sign in the numerator will insure that EKX will be positive. To circumvent the possibility of rounding errors in evaluating

EKX, Eq. [A16] can be rewritten:

$$EKX = -\frac{2 \cdot QC}{QB + (QB^2 - 4 \cdot QA \cdot QC)^{1/2}}. \quad [A17]$$

This essentially concludes the mathematics of the two-site model. There are two additional points that must be addressed to complete the discussion however; the prediction of the transition from one-site to two-site kinetics, and the flux calculation when only one site is active.

First the equation for the one-site flux calculation will be shown. This equation is obtained by solving [A1] with the same boundary conditions as before for $x \to -\infty$ and with the condition given by Eq. [A3] for $x \to 0$. The result is

$$\text{Flux} = \frac{C_{s1} - C_h}{\frac{h}{D} + \frac{1}{(k_1 D')^{1/2}}}. \quad [A18]$$

The conditions under which the transition from one-site to two-site kinetics occurs can be derived by considering Eq. [A1] and [A2]. In these equations x_0 is the position coordinate in the matrix at which the second site begins contributing, because it is only for $x > x_0$ that $C(x)$ is less than C_{s2}. Clearly, the condition necessary for two sites to contribute is that $C(0)$ must be less than C_{s2}. Examination of Fig. 2 leads to the conclusion that when $C(0) = C_{s2}$ then $x_0 = 0$ and when $C(0) < C_{s2}$ then $x_0 < 0$. Hence when $x_0 < 0$ then both sites contribute and the conditions that cause the equality $x_0 = 0$ mark the transition point between one-site and two-site kinetics. Now the conditions required for both sites to be active can be readily determined.

From the definition of EKX it is seen that $x_0 = 0$ implies $EKX = 1$. By rearranging Eq. [A17] it follows that if $EKX = 1$ then $QA + QB + QC = 0$. Substituting the definitions of QA, QB, and QC it can be shown that the transition point is given by

$$h_{tran} = \frac{D(C_{s2} - C_h)}{(k_1 D')^{1/2}(C_{s1} - C_{s2})}. \quad [A19]$$

For h smaller than the transition h (i.e., higher stirring speeds) both sites will contribute, while for larger h only one site contributes. Equation [A19] also shows that for solutions with higher partial saturations (i.e., $C_{s2} - C_h$ smaller) a higher stirring speed is necessary for both sites to participate. Both these observations are in agreement with experimental results obtained for hydroxyapatite.

Now the algorithm for calculating dissolution rate into a given bulk solution at a given rate of rotation of the disk can be readily written.

1. Given K_{HAP1} and K_{HAP2}, calculate C_{s1} and C_{s2}, the apparent solubilities of the sites in the bulk solution.

2. Since the kinetic rate constants for ion disengagement and solution always appear as a product with the diffusivity in the matrix region, these are expressed as single parameters as follows:

$$k_1' = \frac{1}{(k_1 D')^{1/2}} = K1P$$

$$k_2' = \frac{1}{(k_2 D')^{1/2}} = K2P.$$

Now the following quantities are calculated:

$$\begin{aligned} K1PIN &= 1.0/K1P \\ K2PIN &= 1.0/K2P \\ K1DP &= K1PIN^2 \\ K2DP &= K2PIN^2 \\ KSUM &= K1DP + K2DP \\ KSUMRT &= KSUM^{1/2} \\ G &= (K1DP \cdot CS1 + K2DP \cdot CS2)/KSUM \\ T34 &= (CS2 - CS1)/KSUM/2.0 \cdot K1PIN \\ T3 &= T34 \cdot (K1PIN + KSUMRT) \\ T4 &= T34 \cdot (K1PIN - KSUMRT) \end{aligned}$$

3. In general, theoretical dissolution rates will be wanted over a range of rotation

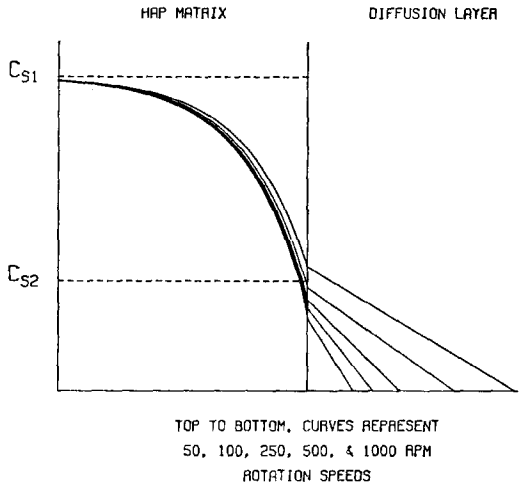

FIG. A1. Concentration profiles as a function of diffusion layer thickness (4% partial saturation).

speeds for each set of bulk solution conditions. For each rotation speed, the diffusion layer thickness, H, is calculated from the Levich equation. The diffusion layer thickness, HTRAN, that marks the transition from one-site to two-site kinetics, is calculated from Eq. [A19]. Now for rotation speeds where H is greater than HTRAN, only one site is active. Otherwise both sites are active.

4. If only one site is active, the flux is given by

$$\text{FLUX} = (CS1 - CH)/(H/D + K1P).$$

If both sites are active, the following procedure is used to calculate the flux:

$$\begin{aligned} DH &= D/H \\ QA &= T4\cdot(DH - K\text{SUMRT}) \\ QB &= DH\cdot(G - CH) \\ QC &= T3\cdot(DH + K\text{SUMRT}) \\ \text{ROOT} &= (QB\cdot QB - 4\cdot QA\cdot QC)^{1/2} \\ EKX &= -2\cdot QC/(\text{ROOT} + QB) \\ Q3 &= T3/EKX \\ Q4 &= T4\cdot EKX \\ \text{FLUX} &= (Q4 - Q3)\cdot K\text{SUMRT} \end{aligned}$$

If H is equal to HTRAN, both procedures will give identical results.

APPENDIX II

Mathematical Properties of the Model and Their Implications

In this appendix we will examine in detail the behavior of the two-site model for a single example set of solution conditions, namely, acetate buffer at pH 4.5 which is 4% saturated with respect to hydroxyapatite and for a range of rotation speeds of the rotating disk. Figure A1 shows the concentration profiles for hydroxyapatite in solution for various speeds of rotation as calculated from the model. C_{s1} and C_{s2} represent the calculated apparent solubilities of the two sites for this set of solution conditions. The topmost profile, corresponding to a slow rotation speed of 50 rpm, is above C_{s2} at all points in the matrix and approaches C_{s1} as the depth into the matrix increases. In this case, site No. 2 will not contribute at all, resulting in strictly site No. 1 dissolution. As the speed of rotation is increased, the diffusion layer thickness is decreased, and the resulting profiles move lower. At the point where these profiles go below C_{s2}, the second site begins contributing. Because the apparent rate constant for the second site is so much larger than that for the first site, this second site will not only become more important as rotation speed increases, but will almost completely determine the total dissolution rate at these higher speeds.

The contributions of each of the sites to the dissolution rate are shown in Fig. A2. The curves labeled "SITE 1" and "SITE 2" show the contributions of these sites to the total dissolution rate as a function of disk rotation. As seen from the profiles in Fig. A1, site No. 2 does not contribute at all at low stirring rates. At the higher rates of stirring the contribution from this site becomes more and more important and eventually exceeds the contribution from site No. 1. The importance of site No. 2 in determining the total dissolution rate is much

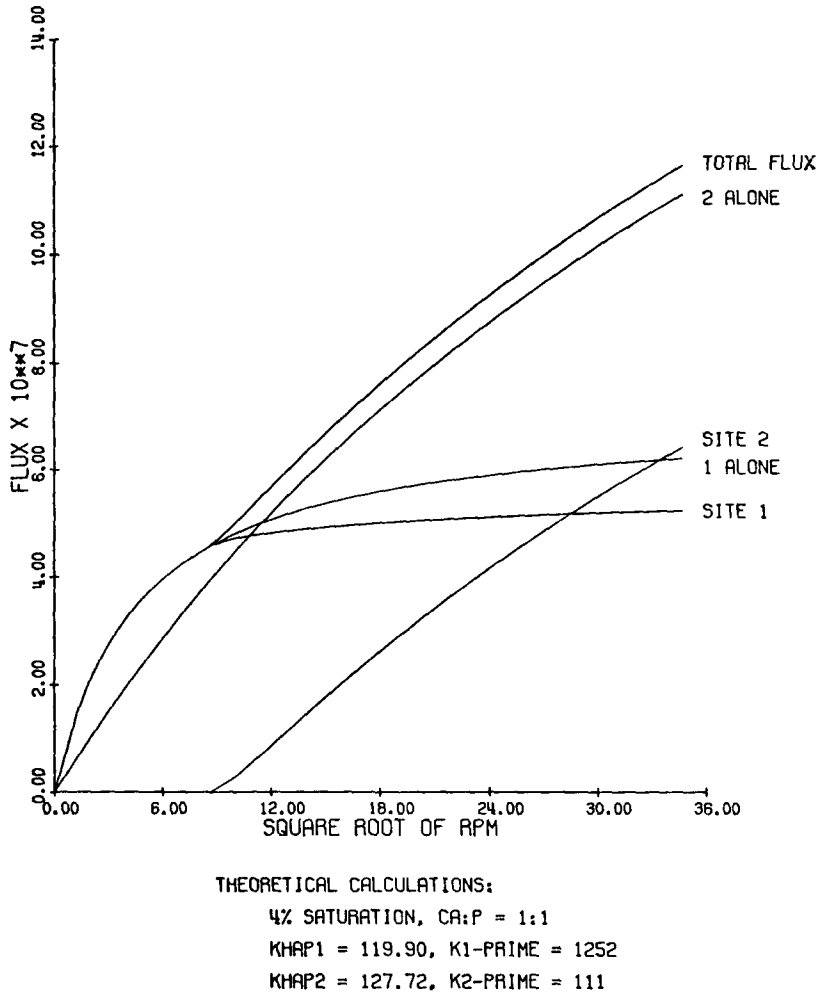

FIG. A2. Contributions of the individual sites to dissolution as a function of disk rotation speed.

greater than is implied by merely comparing the relative magnitudes of the contributions when both sites are operating. The curve labeled "2 ALONE" shows the dissolution that would occur from site No. 2 if Site No. 1 were somehow made inoperative without interfering with the operation of site No. 2. This curve is only a few percent below the curve representing total flux. Hence it is chiefly the properties of site No. 2 that determine the total dissolution rate when conditions are such that this site is operative, even though this site may be contributing less to the total than site No. 1.

On the other hand, if site No. 2 were selectively inhibited so that only site No. 1 were allowed to dissolve, the dependence of total dissolution rate on rotation speed would be that shown by the curve labeled "1 ALONE." Interestingly, White and Nancollas (private communication) have studied the inhibition of hydroxyapatite pellet dissolution by diphosphonates in completely unsaturated solutions, and found that the maximal inhibition attainable is about a 50% reduction in dissolution rate. The dependence on rotation speed observed by these workers is similar to that depicted by the curve labeled "1 ALONE."

This suggests that the diphosphonate

used in the study (HEDP, hydroxyethylidine diphosphonate) selectively inhibits site No. 2, resulting in the rate dependence characteristic of dissolution from site No. 1 only. Griffith *et al.* (46) have recently shown that dissolution of powdered hydroxyapatite in partially saturated buffer solutions where only site No. 1 is active results in the formation of large holes in the crystals, whereas dissolution in completely unsaturated solutions (both sites active) results in no such holes. More recently, Griffith (unpublished) has shown that dissolution in completely unsaturated buffer solutions containing HEDP also results in the hole formation characteristic of dissolution from site No. 1 only, strongly supporting the hypothesis that this agent selectively inhibits site No. 2.

REFERENCES

1. Higuchi, W. I., Gray, J. A., Hefferren, J. J., and Patel, P. R., *J. Dent. Res.* **44,** 330 (1965).
2. Higuchi, W. I., Mir, N. A., Patel, P. R., Becker, J. W., and Hefferren, J. J., *J. Dent. Res.* **48,** 396 (1969).
3. Mir, N. A., and Higuchi, W. I., *Arch. Oral Biol.* **14,** 901 (1969).
4. Fisher, R. B., Muhler, J. C., and Wust, C. J., *J. Dent. Res.* **33,** 50 (1954).
5. McCann, H. G., and Bullock, F. A., *J. Dent. Res.* **34,** 59 (1955).
6. Leach, S. A., *Brit. Dent. J.* **106,** 122 (1959).
7. Malleowalla, A., and Myers, H. M., *J. Dent. Res.* **41,** 413 (1962).
8. Gray, J. A., *J. Dent. Res.* **41,** 633 (1962).
9. Spiers, R. L., Spinelli, M., and Brudevold, F., *J. Dent. Res.* **42,** 811 (1963).
10. Miller, W. D., *J. Brit. Dent. Assoc.* **5,** 104 (1884).
11. Bunting, R. W., and Palmerlee, F., *Proc. Soc. Exp. Biol. N. Y.* **22,** 296 (1925).
12. Enright, J. J., Firesell, H. E., and Trescher, M. O., *J. Dent. Res.* **12,** 759 (1932).
13. Fosdick, L. S., and Wessinger, G. D., *J. Amer. Dent. Assoc.* **27,** 203 (1940).
14. Summerson, W. H., and Neuwirth, I., *J. Dent. Res.* **20,** 157 (1941).
15. Hardwick, J. L., *Brit. Dent. J.* **89,** 1 (1950).
16. Wachtell, L. W., *J. Dent. Res.* **43,** 237 (1964).
17. Noyes, A. A., and Whitney, W. R., *J. Amer. Chem. Soc.* **19,** 930 (1897).
18. Darling, A. I., *Brit. Dent. J.* **101,** 289 (1956).
19. Darling, A. I., *Brit. Dent. J.* **105,** 119 (1958).
20. Darling, A. I., Mortimer, K. V., Poole, D. F. G., and Ollis, W. D., *Arch. Oral Biol.* **5,** 251 (1961).
21. Brudevold, F., *in* "Chemistry and Prevention of Dental Caries" (R. F. Sognnaes and C. C. Thomas, Eds.), Chap. 2, pp. 32–88. Charles C Thomas, Springfield, Illinois, 1962.
22. Gray, J. A., and Francis, M. D., *in* "Mechanisms of Hard Tissue Destruction" (R. F. Sognnaes, Ed.), Publication No. 75, Chap. 8, pp. 213–260. American Association for the Advancement of Science, Washington, D.C., 1963.
23. Gray, J. A., *Arch. Oral. Biol.* **11,** 397 (1966).
24. Sperber, G. H., and Buonocore, M. G., *J. Dent. Res.* **42,** 724 (1963).
25. Wu, M. S., Higuchi, W. I., Fox, J. L., and Friedman, M., *J. Dent. Res.* **55,** 496 (1976).
26. Hodes, B., Ph.D. Thesis, The University of Michigan, Ann Arbor, Michigan, 1972.
27. Levich, V. G., "Physicochemical Hydrodynamics," p. 71. Prentice–Hall, New Jersey, 1962.
28. Fox, J. L., Ph.D. Thesis, The University of Michigan, Ann Arbor, Michigan, 1977.
29. Gilmer, G. H., and Bennema, P., *J. Appl. Phys.* **43,** 1347 (1972).
30. Fawzi, M. B., Fox, J. L., Dedhiya, M. G., Higuchi, W. I., and Hefferren, J. J., *J. Colloid Interf. Sci.* **67,** 304 (1978).
31. Gallily, I., and Friedlander, S. K., *J. Chem. Phys.* **42,** 1503 (1965).
32. Hoffman, S., McEwan, W. S., and Drew, C. M., *J. Dent. Res.* **48**(6) 1234 (1969).
33. Johnson, N. W., Poole, D. F. G., and Tyler, J. E., *Arch. Oral Biol.* **16,** 385 (1971).
34. Nichol, T., Judd, G., and Ansell, G. S., *J. Dent. Res.* **52**(3), 487 (1973).
35. Scott, D. B., Simmelink, J. W., and Nygaard, V., *in* "Chemistry and Physiology of Enamel," pp. 6–24. The University of Michigan Press, Ann Arbor, Michigan, 1971.
36. Swancar, J. R., Scott, D. B., Simmelink, J. W., and Smith, T. J., *in* "Tooth Enamel II" (R. W. Fearnhead and M. V. Stack, Eds.), pp. 233–239. John Wright, Bristol, England, 1971.
37. Johnson, N. W., *Arch. Oral Biol.* **12,** 1505–1521 (1967).
38. Sharpe, A. N., *Arch. Oral Biol.* **12,** 583–592 (1967).
39. Poole, D. F. G., *in* "Tooth Enamel II" (R. W. Fearnhead and M. F. Stack, Eds.), pp. 43–51. John Wright, Bristol, England, 1971.
40. Arends, J., Berg, v. d. P. J., and Jongeblood, W. L., *in* "Physicochimie et Cristallographie des Apatites d'interet Biologique," pp. 389–395. Proceedings of Colloques Internationaux C.W.R.S., 1975.
41. Arends, J., *Caries Res.* **7,** 261–268 (1973).
42. Johansen, E., *in* "Tooth Enamel" (M. V. Stack and R. W. Fearnhead, Eds.), pp. 177–184. John Wright, Bristol, England, 1965.

43. Nylen, M. V., Eanes, E. D., and Omnell, K., *J. Cell Biol.* **18,** 109–124 (1963).
44. Ronnholm, E., *J. Ultrastruct. Res.* **6,** 249–303 (1962).
45. Selvig, K. A., *Calif. Tiss. Res.* **6,** 227–238 (1970).
46. Griffith, E., Katdare, A., Fox, J. L., and Higuchi, W. I., *J. Colloid Sci.*, **67,** 331 (1978).
47. Koulourides, T., Feagin, F., and Pigman, W., *Arch. Oral Biol.* **13,** 335–341 (1968).
48. Feagin, F., Patel, P. R., Koulourides, T., and Pigman, W., *Arch. Oral Biol.* **16,** 535–548 (1971).
49. Koulourides, T., Ceuto, H., and Pigman, W., *Nature (London)* **189,** 226 (1961).
50. Koulourides, T., Feagin, F., and Pigman, W., *Ann. N. Y. Acad. Sci.* **131,** 751–757 (1965).
51. Pigman, W., Kotwal, K., and Koulourides, T., *Arch. Oral Biol.* **11,** 815–824 (1966).
52. Koulourides, T., *in* "Chemistry and Physiology of Enamel," pp. 109–119. The University of Michigan Press, Ann Arbor, Michigan, 1971.
53. Brown, W., "Physicochemical Aspects of Decay and Decalcification." NBS Report 10378, National Bureau of Standards, Washington, D.C., 1970.